



Data-driven model reduction for fast temperature prediction in a multi-variable data center

Shu-Qi Jin^a, Nan Li^a, Fan Bai^a, Yu-Jie Chen^b, Xiang-You Feng^a, Hao-Wei Li^a,
Xiao-Ming Gong^a, Wen-Quan Tao^{a,*}

^a Xi'an Key Laboratory of Energy Saving and Low Carbon Technology of Data Center, Key Laboratory of Thermal Fluid Science and Engineering of MOE, School of Energy and Power Engineering, Xi'an Jiaotong University, Xi'an, Shaanxi 710049, PR China

^b School of Mechanical Engineering, Beijing Key Laboratory of Pipeline Critical Technology and Equipment for Deepwater Oil & Gas Development, Beijing Institute of Petrochemical Technology, Beijing 102617, China

ARTICLE INFO

Keywords:

Data center
CFD simulation
Reduced order model
Data-driven method
Fast temperature field prediction

ABSTRACT

With the rapid development of digital economy, the number of data centers and their capacity have been increasing sharply, and data center energy consumption becomes a whole-society concern. Computational fluid dynamics (CFD) is currently widely used to obtain the thermal fields inside air-cooled data centers to enable design improvements and optimize the airflow organization. However, a CFD simulation needs a lot of time which can not be accepted for real-time operation. In the present study, a design tool called pairwise independent combinatorial testing (PICT) is applied to optimize the simulation conditions and to maximize the amount of useful information obtained with the minimum number of numerical tests. Based on the snapshots, the proper orthogonal decomposition (POD) method combined with the multivariate adaptive regression splines (MARS) method, is proposed and used in a real row-level data center of 199 independent variables. Under design conditions, POD-MARS predictions are in good agreement with CFD simulations with the average mean relative error for 20 tested cases being $\sim 0.01\%$. For another 20 randomized cases under off-design conditions, the average mean relative error is 6.45%, the corresponding mean absolute error is 1.89 °C and on average there is 92.36% area of the total three-dimensional temperature field where the relative error doesn't exceed 15%. The POD-MARS computation takes only 30s to obtain a 3D temperature field for the same test case which is ~ 240 times faster than CFD simulation on the same desktop computer.

1. Introduction

Data centers (DC) undertake the responsibility of transmitting, processing, computing, and storing data information of society. With the urgent demand for the digital economy and 5G communications, the number of data centers has been increasing rapidly and their power consumption has reached about 2% of the total power consumption of society, becoming a high-energy consumption industry [1]. Energy saving is a critical challenge faced by the community of worldwide data centers. The energy consumption in data centers usually consists of IT equipment, cooling system, power supply system, and others. Among all the factors, the energy consumption of the cooling system accounts for about 40% [2]. Therefore, energy reduction for cooling systems is one of the main routes for energy saving in data centers.

Reasonable airflow organization is an effective way to reduce energy

consumption and upgrade energy utilization efficiency [3]. Now there are two common structures of the air-cooled data centers, room-level with raised floor and row-level with non-raised floor. Numerical simulation (CFD/NHT) is usually applied to get a better airflow organization inside the data center, and the computed temperature and velocity field distributions are used to comprehensively evaluate the thermal environment of the data center [4–6]. The simulation results also help to optimize the capacity configuration, equipment selection, structural transformation, etc. [7–11].

Whereas, the CFD/NHT simulation for a practical data center (hundreds of cabinets and even more) needs to generate millions of to tens of millions of grid cells for accuracy, and the computation times needed usually range from several hours to days which is far from meeting the requirement of real-time control. To acquire the data center thermal environment as soon as possible, researchers have made some efforts to investigate fast and efficient prediction approaches including response

* Corresponding author.

E-mail address: wqtao@mail.xjtu.edu.cn (W.-Q. Tao).

Nomenclature

Uppercase letters

ACU	Air-conditioning unit
$B_{i, obs}$	Observed weighting coefficient
DC	Data center
J	Jacobi matrix
T	Temperature
T_0	Mean temperature
U	Left singular vector
V	Right singular vector

Lowercase letters

b_i	Weighting coefficient for a new test
h	Core matrix

Greek symbols

σ	Singular value
ψ	POD mode

Subscripts

E	Error in absolute temperature
k	Truncation order
m	Number of cell nodes
n	Number of snapshots
R	Relative temperature difference

Superscript

T	Transpose
-----	-----------

Galerkin projection method. Samadiani and Joshi [20,21] made the first attempt to apply this reduced order method, the POD model, in a simplified small data center of 8 racks and 1 computer room air conditioning (CRAC) unit. To reduce the number of design variables for illustration, 5 design variables were selected which contain the rack heat loads and CRAC airflow rate where the corresponding racks in each column have the same heat load. These 5 parameters are varied to generate 19 or 21 observed temperature fields of simulation results for the case studied. Later, Samadiani et al. [22] utilized selected 7 sets of observed thermal sensor data inside an operational data center to help the prediction of the temperature field as a function of the airflow rate of one CRAC unit, which is the only control parameter. Ghosh and Joshi [23] used the POD-interpolation method for rapid temperature prediction in a data center with 3 CRACs and 10 racks arranged in a 5×2 alternating cold/hot aisle arrangement. Phan and Lin [24] generated a 3-D temperature profile of the data center model using the POD method, while this profile was constructed from 2D slices with a linear interpolation technique for two-parameter and three-parameter observations. The same data center model was adopted from the one that has been used by previous studies by other researchers [25,26]. Fouladi et al. [27] proposed a novel hybrid modeling strategy by using the POD method for room airflow modeling and the flow network modeling for external components to save energy and exergy in data centers. In the following literatures more applications of data-driven method for data centers can be found. Athavale et al. [28] compared the performance of three different data-driven methods, namely artificial neural networks (ANN), support vector regression (SVR), Gaussian process regression (GPR) with POD model in predicting both steady-state and transient-state rack inlet air temperature distributions in data centers. For the steady-state prediction, the models were trained on the results from 300 CFD/HT simulation results and it is found that the accuracy of these modeling is

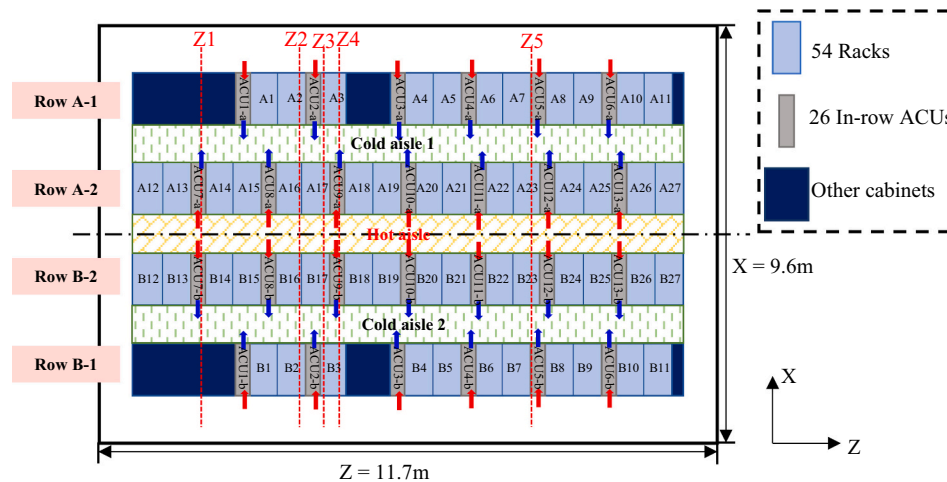


Fig. 1. The overview of the studied data center.

surface methodology [12], potential flow methods [13,14], proper orthogonal decomposition (POD), etc. The POD method was first introduced into fluid mechanics by Lumley [15] for the analysis of coherent structure in turbulent flows. Ding et al. [16] utilized this method for the fast and accurate predictions of velocity and temperature fields in the fundamental fluid flow and heat transfer issues. Han et al. [17] applied POD reduced-order model for steady-state natural convection based on a body-fitted coordinate system and the velocity and temperature fields are generated. Chen et al. [18] established POD reduced-order model for isotropic turbulent flow of viscoelastic fluid for the first time. Li et al. [19] established a global reduced-order model for the steady-state flow in fractured porous media based on the embedded discrete fracture model by using the POD method combined with

impacted by the size of trained dataset. An ANN with the rectified linear Unit activation function was used to predict pressure distributions in a row-based cooling data center with three variables by Asgari et al. [29]. The cooling unit operation and server workload varied to reveal their influences on the thermal performance of the DC. Asgari et al. [30] developed a gray-box model that combined machine learning with the thermo-fluid transport equations relevant for a row-based cooled data center with CPU temperature measured by sensors. Phan and Lin [31] proposed the response surface methodology (RSM) based on the radial basis function (RBF) for rapid thermal simulation and optimal design of data centers. Three parameters were studied and the results significantly reduced the running time while maintaining a good accuracy.

All the above studies provided ideas for rapid temperature prediction

Table 1
IT Equipment list for all racks.

Rack ID	equipment quantity divisions	Number of effective variables	Rack ID	equipment quantity divisions	Number of effective variables
A1	10-2-10	3	B1	10-2-10	3
A2	10-2-10	3	B2	10-1-10	3
A3	10-3-10	3	B3	0-0-0	0
A4	10-2-9	3	B4	10-2-10	3
A5	10-1-9	3	B5	10-1-10	3
A6	10-2-8	3	B6	10-2-10	3
A7	10-1-10	3	B7	10-1-10	3
A8	10-2-10	3	B8	10-2-10	3
A9	10-1-10	3	B9	10-1-10	3
A10	10-2-10	3	B10	10-2-10	3
A11	10-1-10	3	B11	10-1-10	3
A12	0-2-0	1	B12	10-2-10	3
A13	0-1-0	1	B13	10-1-10	3
A14	0-2-0	1	B14	10-2-10	3
A15	10-1-10	3	B15	10-1-10	3
A16	10-2-10	3	B16	10-2-10	3
A17	10-1-10	3	B17	10-1-10	3
A18	10-2-10	3	B18	10-2-10	3
A19	10-1-10	3	B19	10-1-10	3
A20	10-2-10	3	B20	10-2-10	3
A21	10-1-10	3	B21	10-1-10	3
A22	10-2-10	3	B22	10-2-10	3
A23	10-1-10	3	B23	10-1-10	3
A24	0-2-0	1	B24	10-2-10	3
A25	0-1-0	1	B25	10-1-10	3
A26	0-2-0	1	B26	10-2-10	3
A27	10-1-10	3	B27	10-1-10	3

Total number of effective variables for all racks: 147.

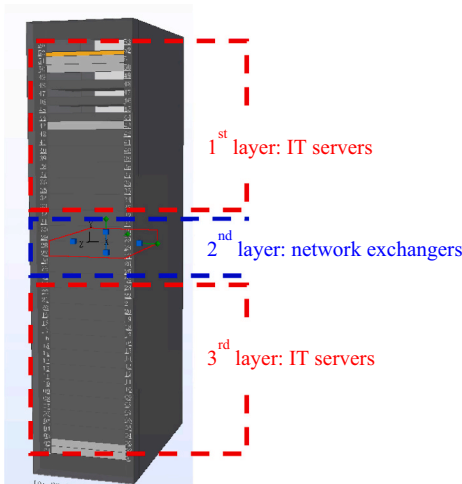


Fig. 2. Scheme of a 3-layer classification method for racks.

Table 2
Variable description.

IT Equipment type	Power density per unit (W)	Supply air temperature (°C)	Volume flow rate (m ³ /h)	Number of variables
1st layer servers	0-400	-	-	147
2nd layer network exchangers	0-350	-	-	
3rd layer servers	0-400	-	-	
In-row air conditioning	-	15-27	0-5100	2*26 = 52

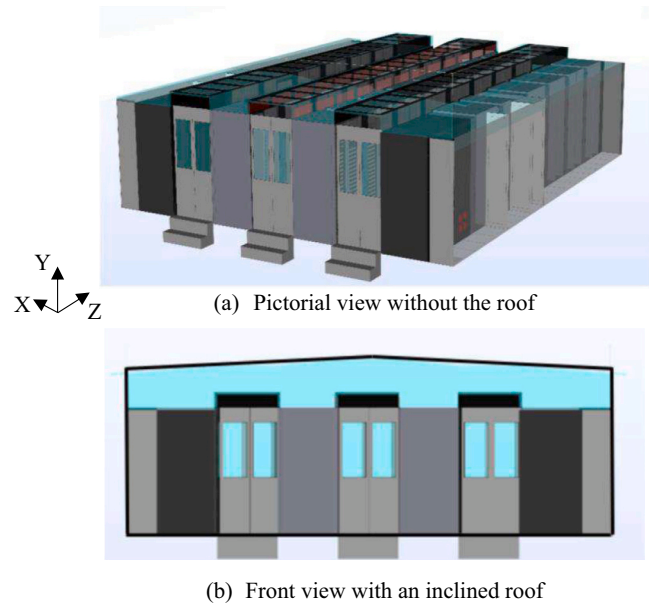


Fig. 3. The numerical model of the studied data center.

in data centers. However, they are all limited by the capacity of data centers and the number of investigated variables. The maximum number of racks of the above studies is 28 and the controlling variables are usually <2 or 3 parameters. For the application in real data centers, where there are hundreds or even more racks and hundreds of changeable parameters, two main challenges exist, i.e., how to design experiment/simulation conditions and how to balance the computational time and accuracy.

In the present study, the reduced order model combined with the data-driven method is applied to a real data center room with 54 racks and 199 multi-variables for rapid temperature field prediction. The rest of the paper is organized as follows. In Section 2, the physical model of the studied data center and its numerical solutions are introduced. The detailed procedure and methodology of the POD model combined with the data-driven method are explained in Section 3. The predicted results of temperature field are verified and reviewed in Section 4. Finally, some important conclusions and findings are summarized in Section 5.

2. Physical and numerical models of the studied data center

2.1. Physical model and variables

The physical model is a real row-level data center with 9.6m (length, X) × 11.7m (width, Z) × 3.65 (height, Y) and an inclined roof, containing 54 racks and 26 in-row air-conditioning units (ACU) as shown in Fig. 1. As can be seen from the figure, the racks are arranged in four rows symmetrically with the horizontal axis of the room. The three aisles are isolated with one being hot and the other two being cold. Besides, 10 more cabinets for the electric power system and fire-extinguishing system storage are planted in the corner of the DC room. The in-row air-conditioning unit of 1.2m × 0.3m × 2.5m is planted generally between every two racks.

Each rack has a size of a length of 1.2 m and a height of 2.5 m. On average, each rack consists of twenty 2-unit (U) servers from bottom to top and two 1-U network exchangers in the middle for the connection, and there are 1017 IT equipment in total. For each server, the power varies from 50 W to 400 W, and for each network exchanger from 50 W to 300 W. The diverse power load among different racks makes the problem very challenging. Thus, we adopt a 3-layer classification method for racks according to the IT equipment list shown in Table 1 (see Fig. 2). Among 54 racks, no servers are installed in racks A12-14,

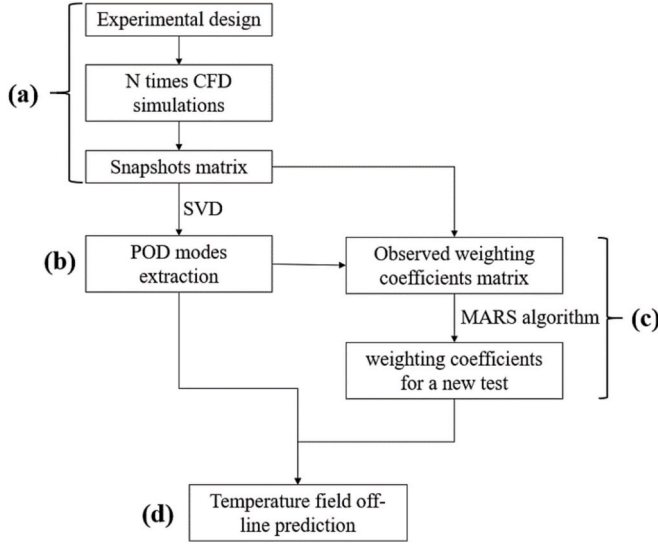


Fig. 4. Flow chart of the computation process.

A24–26 and B3. The equipment quantity divisions in the table represent the number of server/ network exchangers of a layer and it is assumed that the power density of each layer is distributed uniformly. In this way, the number of variables for rack power density is accounted as 147. There are two control parameters for every in-row ACU, that is, supply air with temperature from 15 °C to 27 °C and volume flow rate between 0 and 5100 m³/h which are listed in Table 2. Hence, the number of variables for 26 ACUs is 52 in total. The total number of variables is 199 in the present paper as listed in Table 2.

2.2. Numerical model

As indicated in Section 2.1, the simulated data center is a row-level one, which means the cold air is supplied by the ACUs located within racks. In Fig. 1, the blue arrows show the cold air outlet from the ACUs and the red arrows show the inlet of hot air to the ACUs. The ACUs provide a constant flow rate of air at a specified air supply temperature.

A numerical model of the above structure is built as shown in Fig. 3. A stepwise approximation is applied in the simulation to the inclined roof. In the model, the rack is considered as the server-level black-box model with a uniform load of each layer. The server is modeled as a hollow cube by specifying a fixed power and the mass flow rate is determined by the specific server type and its characteristic curve. The walls of all the cabinets are modeled as adiabatic surfaces with zero velocity.

2.2.1. Assumptions and governing equations

The following assumptions are made in the simulation: (1) Air is regarded as an incompressible fluid, and the flow is turbulent and steady; (2) The effects of radiation and natural convection are ignored; (3) The data center space is air tightness without exterior windows.

In data centers, airflow is usually turbulent, according to previous studies [32,33], the k-ε turbulence model with standard wall functions works well and they are adopted in this study. The governing equations of mass conservation, momentum conservation, and energy conservation are listed below.

Mass conservation:

$$\frac{\partial u}{\partial x} + \frac{\partial v}{\partial y} + \frac{\partial w}{\partial z} = 0 \quad (1)$$

Momentum conservation:

$$\frac{\partial(uu)}{\partial x} + \frac{\partial(vu)}{\partial y} + \frac{\partial(wu)}{\partial z} = -\frac{1}{\rho} \frac{\partial p}{\partial x} + \nu \left(\frac{\partial^2 u}{\partial x^2} + \frac{\partial^2 u}{\partial y^2} + \frac{\partial^2 u}{\partial z^2} \right) \quad (2)$$

$$\frac{\partial(uv)}{\partial x} + \frac{\partial(vv)}{\partial y} + \frac{\partial(wv)}{\partial z} = -\frac{1}{\rho} \frac{\partial p}{\partial y} + \nu \left(\frac{\partial^2 v}{\partial x^2} + \frac{\partial^2 v}{\partial y^2} + \frac{\partial^2 v}{\partial z^2} \right) \quad (3)$$

$$\frac{\partial(uw)}{\partial x} + \frac{\partial(vw)}{\partial y} + \frac{\partial(ww)}{\partial z} = -\frac{1}{\rho} \frac{\partial p}{\partial z} + \nu \left(\frac{\partial^2 w}{\partial x^2} + \frac{\partial^2 w}{\partial y^2} + \frac{\partial^2 w}{\partial z^2} \right) \quad (4)$$

Energy conservation:

$$\frac{\partial(uT)}{\partial x} + \frac{\partial(vT)}{\partial y} + \frac{\partial(wT)}{\partial z} = a \left(\frac{\partial^2 T}{\partial x^2} + \frac{\partial^2 T}{\partial y^2} + \frac{\partial^2 T}{\partial z^2} \right) + S \quad (5)$$

k-ε turbulence model:

$$\frac{\partial k}{\partial t} + U_j \frac{\partial k}{\partial x_j} = \tau_{ij} \frac{\partial U_i}{\partial x_j} - \varepsilon + \frac{\partial}{\partial x_j} \left[\left(\nu + \frac{\nu_T}{\sigma_k} \right) \frac{\partial k}{\partial x_j} \right] \quad (6)$$

$$\frac{\partial \varepsilon}{\partial t} + U_j \frac{\partial \varepsilon}{\partial x_j} = C_{\varepsilon 1} \tau_{ij} \frac{\partial U_i}{\partial x_j} - C_{\varepsilon 2} \frac{\varepsilon^2}{k} + \frac{\partial}{\partial x_j} \left[\left(\nu + \frac{\nu_T}{\sigma_\varepsilon} \right) \frac{\partial \varepsilon}{\partial x_j} \right] \quad (7)$$

2.2.2. Boundary condition and grid system

The inclined roof and all other outside boundaries of the computational domain are regarded as the adiabatic boundary with zero velocity.

The grid numbers along the X, Y, and Z directions are 113, 85, and 294, respectively. The total number of grid cells is 2823870. As far as the grid independence of the numerical results is concerned, we have carefully compared our case with Reference [19]: the number of racks and the volume of the studied data center in [19] are 8 and 81m³, respectively, while a mesh with 431,120 cells is considered fine enough compared with 334,972 and 182,000 cells. In our study, the number of racks is 54 which is 6.75 times of the former, the volume of the studied data center is 410 m³ which is 5.06 times of [19], and the 2,823,870 cells are nearly 6.55 times of 431,120. Therefore it is believed that our mesh is fine enough to get grid-independent solutions. The convergence criteria of the iterative solution process are set as the mass and momentum residuals being <10⁻⁵. Usually, 1000 iterations are needed to reach the convergence criteria.

The above governing equations are discretized by the finite volume method and the commercial software 6SigmaDC is adopted for simulation. The default settings of the numerical scheme in the 6SigmaDC are applied.

3. Methodology on data-driven model reduction

The numerically simulated results are used as a dataset in the reduced-order model treatment. The reduced order model for temperature field prediction in the present study is the proper orthogonal decomposition (POD), which is proposed by Hotelling [34] in 1933, and is also known as Karhunen-Loève decomposition (KLD) in signal processing [35] and the principal component analysis (PCA) in statistics [36]. POD is a powerful and efficient method for the treatment of data which are fields like temperature, velocity, etc.. It projects the original data in a high-dimensional space on a new set of basic functions in a low-dimensional space and maintains information of high-dimensional data as much as possible. The implementation of the temperature prediction in the present study follows the four steps outlined in Fig. 4: (a) Prepare the experimental design and snapshots collection. It should be noted that the ‘experimental design’ here is an idiomatic usage, which actually means the design of control parameters for simulations. In this paper the word experimental should be regarded in this way; (b) Calculate the POD modes; (c) Compute the weighting coefficient; (d) Generate the temperature field.

In this study, the data sets are generated from offline CFD simulations with multiple variables varying in prespecified ranges. From CFD

Table 3
Control parameters and level settings for experimental design.

level	Control parameter							
	Parameters for racks:147						Parameters for ACUs:26*2 = 52	
	10 servers (W)	9 servers (W)	8 servers (W)	3 switches (W)	2 switches (W)	1 switch (W)	Volume flow rate (m ³ /h)	Supply air temperature (°C)
1	0	0	0	0	0	0	0	15
2	175	150	140	250	150	75	300	16
3	350	300	280	450	300	150	600	17
4	525	450	420	650	450	225	900	18
5	700	600	560	900	600	300	1200	19
6	875	750	700				1500	20
7	1025	900	840				1650	21
8	1200	1050	980				1800	22
9	1375	1200	1120				1950	23
10	1550	1350	1260				2100	24
11	1725	1500	1400				2250	25
12	1900	1650	1540				2400	26
13	2075	1800	1680				2550	27
14	2350	1950	1820				2700	
15	2525	2100	1960				2850	
16	2700	2250	2100				3000	
17	2875	2400	2240				3150	
18	3050	2600	2380				3300	
19	3225	2800	2520				3450	
20	3400	3000	2700				3600	
21	3600	3200	2900				3750	
22	3800	3400	3050				3900	
23	4000	3600	3200				4150	
24							4400	
25							4750	
26							5100	

Table 4
Partial variable list for experimental design of the snapshots.

No.	Factor	
1		1st layer power density (W)
2	A1	2nd layer power density (W)
3		3rd layer power density (W)
4		1st layer power density (W)
5	A2	2nd layer power density (W)
6		3rd layer power density (W)
...
145		1st layer power density (W)
146	B27	2nd layer power density (W)
147		3rd layer power density (W)
148		Volume flow rate (m ³ /h)
149	ACU-1a	Supply air temperature (°C)
...
198		Volume flow rate (m ³ /h)
199	ACU-13b	Supply air temperature (°C)

simulation, snapshots under design conditions are prepared and step (b) in Fig. 4 is conducted. After finishing step (c), the temperature field can be numerically reconstructed on the POD modes by the following equation (step (d)):

$$T = T_0 + \sum_{i=1}^k b_i \psi_i \quad (8)$$

where T_0 is the mean temperature matrix of each grid cell of all the snapshots; the POD mode, ψ_i , is calculated according to the results of simulation snapshots using the SVD method (step (b)); the weighting coefficient for a new test, b_i , is calculated using the data-driven method (step (c)); and k is the truncation order of the POD modes obtained after decomposition ($1 \leq k \leq n - 1$). The details of implementing each step in Fig. 4 are explained in the following sub-sections.

3.1. Experimental design and snapshots collection

Before the generation of snapshots, it is necessary to design the operating conditions for each snapshot. Experimental design is an efficient way of optimizing the experimental conditions to maximize the amount of useful information obtained with the minimum number of experiments. In the experimental design, the parameters that affect the experimental indicators are called factors, and the number of values that can be set for each parameter is called the level. There are a variety of experimental design methods, including full factorial design [37], orthogonal experimental design [38], pairwise testing [39], uniform design [40], etc.

As indicated in the Introduction, to the authors' knowledge, so far the maximum number of racks for POD studies is only 28 and the control variables are usually several parameters. However, in this study, the number of racks is 59 and the controlling variables are 199. All the above-mentioned experimental design methods can not be used for such a large number of variables and their different levels. After an extensive literature search, it's found that only the pairwise testing method can be applied and the test configuration design tool developed by Microsoft, Pairwise Independent Combinatorial Testing (PICT) is adopted. According to the IT equipment arrangement in Table 1, the first and third layers for each rack consist of servers, while the second layer consists of network exchangers that connect tens of servers through the network. According to the studied data center, the power load for the first and third layers is modulated at steps of about 140-175 W and the second layer at steps of 75-250 W. The corresponding number of levels for the 1st/3rd layer is 23 and for the 2nd layer is 5, and the power load density of each level for different racks is assumed uniform. As for the ACUs, the number of levels for volume flow rate and supply air temperature is set as 26 and 13 respectively. The volume flow rate of the ACU designed by the manufacturer is between 1500 m³/h and 4000 m³/h, and the starting and ending levels of the ACU flow rates are set as 0 and 5100 m³/h, respectively. The detailed level settings for each control parameter are listed in Table 3. Combining with the IT equipment list in Table 1, the total 199 variables are selected and partially listed in

Table 5
Examples of the operating conditions of the snapshots.

No.Variable No. snapshot	1	2	3	...	145	146	147	148	149	...	198	199
1	3400	300	2700	...	1725	150	1725	2100	19	...	2250	22
2	875	0	2525	...	2700	0	525	2550	26	...	2550	26
3	2875	600	1200	...	3050	225	3600	3150	20	...	4400	25
4	1375	450	1025	...	875	75	2525	2850	15	...	3300	15
5	350	150	350	...	1200	300	3800	1500	21	...	2850	16
6	3225	600	3050	...	1375	300	2350	2250	16	...	3450	23
7	1200	450	525	...	3225	150	2700	1950	22	...	3600	17
8	3800	300	2875	...	2075	75	1375	2400	18	...	2700	18
9	4000	150	175	...	175	0	175	1650	23	...	2400	24
10	1025	0	700	...	3600	225	4000	5100	17	...	3000	21
.....
1819	875	300	2525	...	2875	150	1900	0	19	...	1800	15

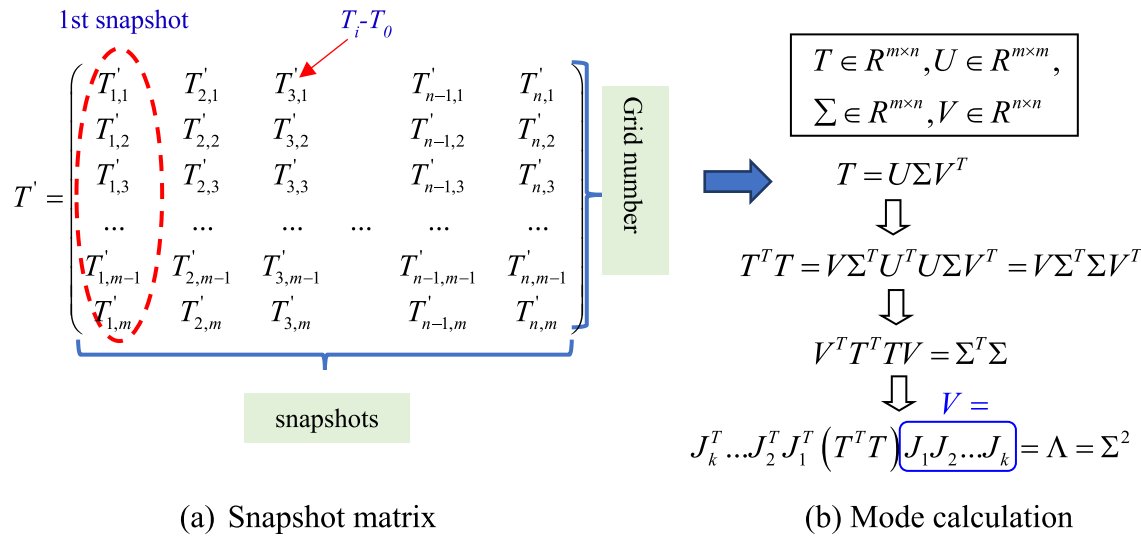


Fig. 5. Snapshot matrix and flowchart of POD modes calculation.

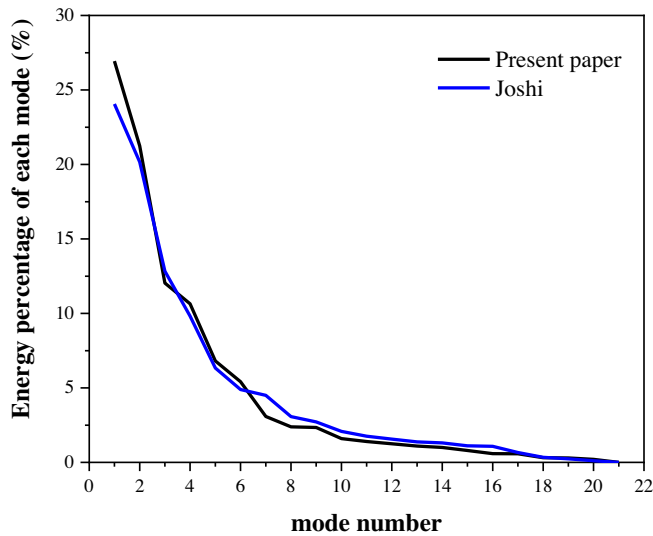


Fig. 6. Verification of POD mode computation with literature.

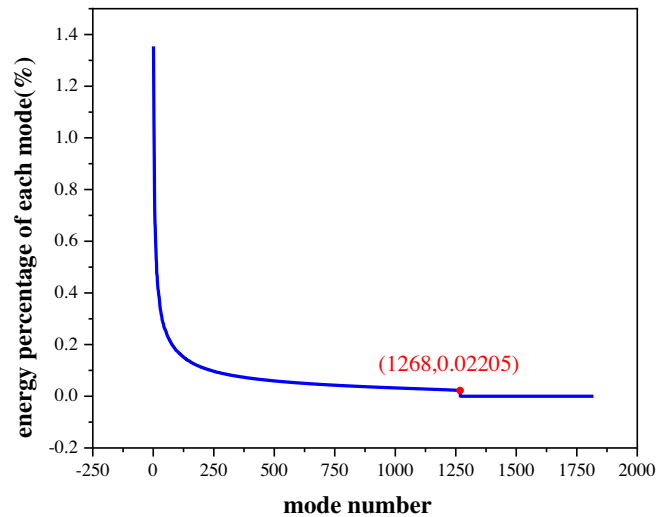


Fig. 7. Energy percentage captured by each POD mode.

Table 4 which exhibits the parameter conditions for the experimental design.

Finally, 1819 snapshots are selected from the design results of PICT, as schematically shown in Table 5, and details are provided in Appendix

1.

3.2. POD modes calculation based on the snapshots

After carrying out the CFD simulations of the snapshots, their tem-

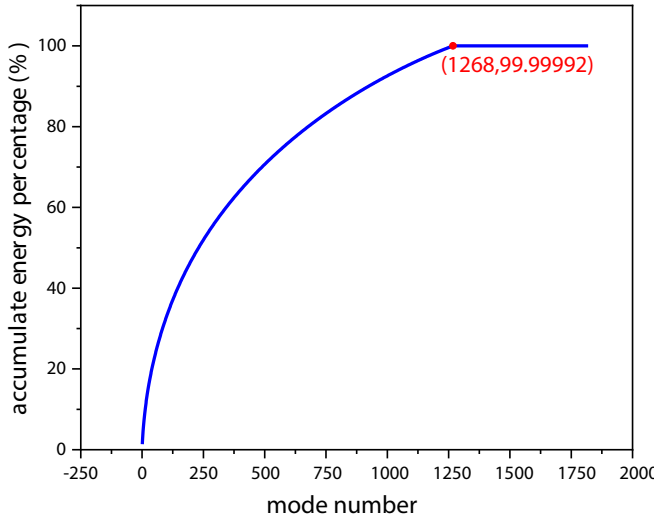


Fig. 8. Accumulate energy percentage of POD modes.

perature matrix can be computed and constructed. Before the POD calculation, we make centralized data preprocessing of the snapshots, that is, the grid temperature of each snapshot is subtracted from the average grid temperature of all the snapshots (denoted by $T_0(x,y,z)$) as shown in Eq. (9). The resulted temperatures of each snapshot are stored in a column vector with m entries. All snapshots of the system under consideration are stored in a rectangular $m \times n$ matrix as a database (Fig. 5).

$$T'(x_i, y_i, z_i) = T(x_i, y_i, z_i) - T_0(x, y, z) \quad (9)$$

In the present study, POD modes are extracted using singular value decomposition (SVD) that generalizes the eigendecomposition of a square normal matrix with an orthonormal eigenbasis for this $m \times n$ matrix. It should be noted that the transpose of a matrix, instead of the

conjugate transpose, is applied in this study because the values are all real numbers. Specifically, the real $m \times n$ matrix of the temperature snapshot is factorized in the following form by SVD:

$$T = U\Sigma V^T \quad (10)$$

where U is an $m \times m$ real orthogonal matrix called left singular vector, Σ is an $m \times n$ rectangular diagonal matrix with non-negative real numbers on the diagonal as shown in Eq. (11), and V is an $n \times n$ real orthogonal matrix called right singular vector.

$$\Sigma = \text{diag}(\sigma_1, \sigma_2, \sigma_3, \dots) \quad (11)$$

The diagonal entries σ_i in Eq.(11) are called the singular values of the real matrix T and they satisfy $\sigma_1 \geq \sigma_2 \geq \sigma_3 \geq \dots \geq \sigma_i$. The matrix U and matrix V satisfy $U^T U = I$, $V^T V = I$, respectively. POD modes can be written as the linear transformation of the snapshots by right singular vectors, as shown in Eq.(12)

$$\psi_{m \times n} = T_{m \times n} V_{n \times n} \quad (12)$$

In this study, the singular value decomposition (SVD) is utilized to decompose the snapshot matrix and the Jacobi algorithm [41] is adopted for this purpose. The right singular vector ($V_{n \times n}$) is decomposed by a series of Jacobi transformations, as shown in Eq. (13),

$$V = J_1 J_2 \dots J_n \quad (13)$$

The implementation steps of Jacobi algorithm are as follows:

- (a) Calculation of the initial core matrix h from the known temperature matrix

$$h = T^T T \quad (14)$$

- (b) Calculation of the second-order principal submatrix of core matrix

$$\begin{pmatrix} h_{m,m} & h_{m,n} \\ h_{n,m} & h_{n,n} \end{pmatrix} \quad (15)$$

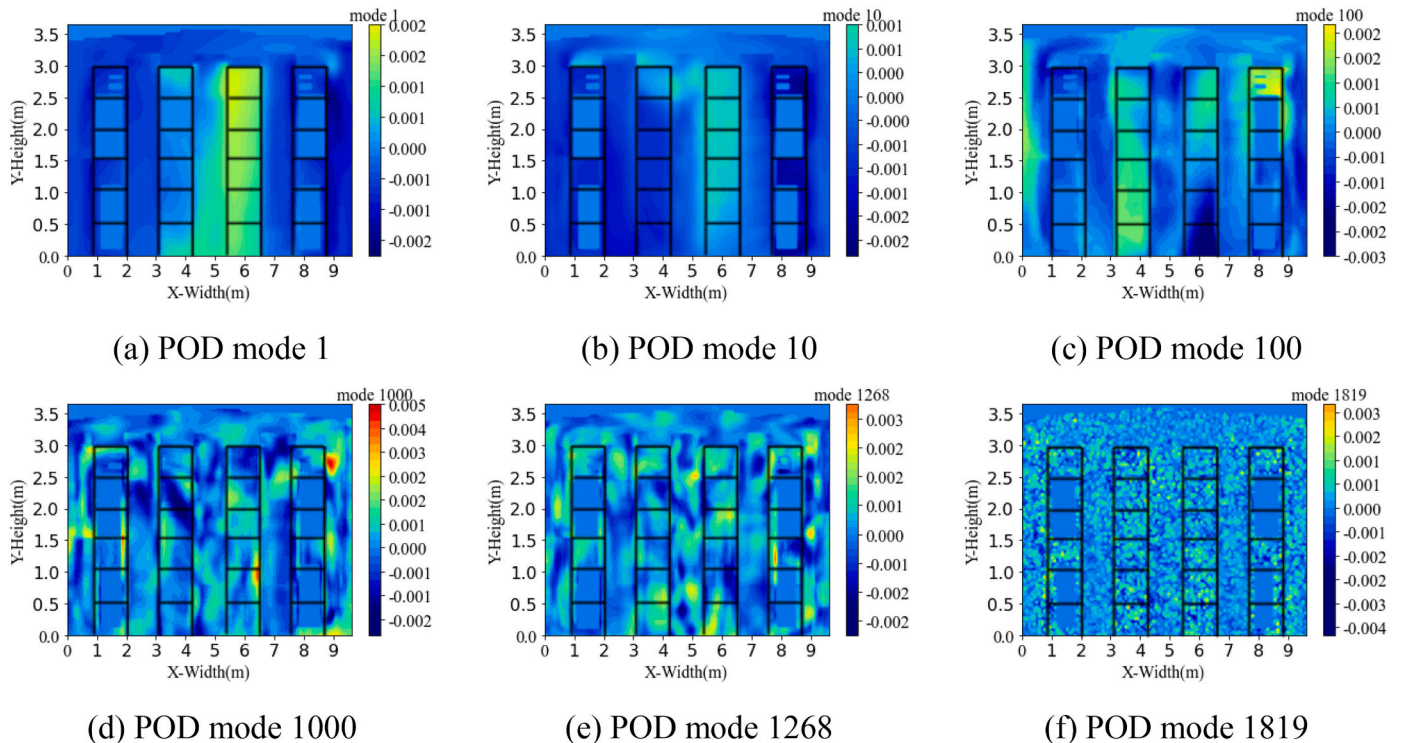


Fig. 9. Contours of POD mode 1,10,100,1000,1268,1819 for temperature field at $Z2 = 3.58$ m.

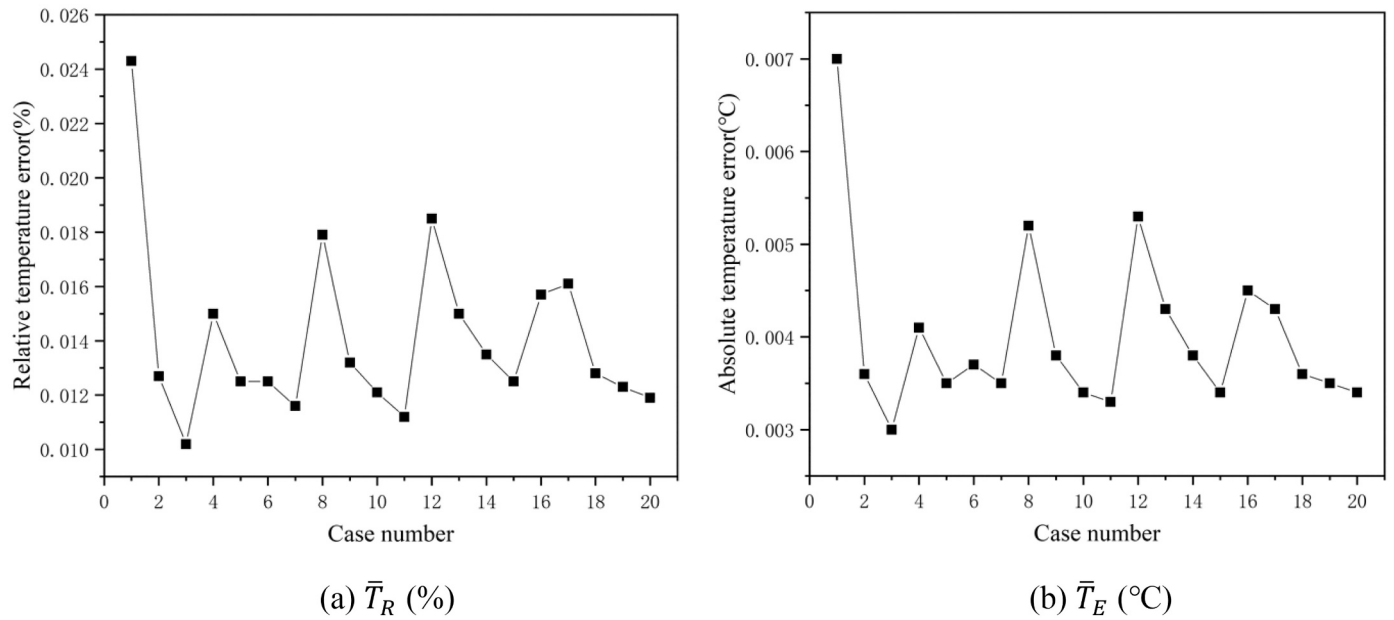


Fig. 10. Results of \bar{T}_R and \bar{T}_E of 20 design conditions.

(c) Calculation of Jacobi matrix

$$\tau = \frac{h_{m,m} - h_{n,n}}{h_{m,n} + h_{n,m}}, t = \frac{\text{sign}(\tau)}{|\tau| + \sqrt{1 + \tau^2}}, c = \frac{1}{\sqrt{1 + t^2}}, s = tc \quad (16)$$

The k^{th} Jacobi matrix is defined as:

$$J_{k(m,m)} = J_{k(n,n)} = c, J_{k(n,m)} = -J_{k(m,n)} = s \quad (17)$$

(d) Update of core matrix:

$$h' = J_k^T h J_k \quad (18)$$

(e) Loop of steps (b) ~ (d) until the core matrix is transformed to a diagonal matrix and the following formula holds:

$$J_n^T \dots J_2^T J_1^T h J_1 J_2 \dots J_n = V^T T^T T V = \Lambda = \sigma^2 \quad (19)$$

(f) Calculation of the right singular vector V defined in Eq. (13).

(g) Determine POD modes by substituting Eq. (13) into Eq. (12).

(h) Normalization of each POD mode as shown in Eq. (20).

$$\psi_i = \frac{\psi_i}{\|\psi_i\|_2} \quad (20)$$

where $\|\psi_i\|_2$ is the norm of the mode ψ_i .

(i) Calculation of singular value (σ_i) according to Eq. (19). The singular value will be used in the later discussion.

3.3. Weighting coefficient prediction for a new case

Generally, there are three methods to generate weighting coefficients b_i for a new case with off-design conditions, which are the Galerkin projection method [16], the interpolation method [22], and the machine learning regression method proposed in this paper. This step is essential to create a reduced-order thermal/fluid model as shown by Eq. (8).

In the first method, the Galerkin projection of the POD modes onto the governing equations results in a set of algebraic equations to be solved for the POD weighting coefficients. The previous investigations using this method are all for simple geometries such as the lid-driven cavity flow and natural convection in a cavity [16], where boundary conditions are easily described by the inclusion of a source term in the decomposition. However, for a complicated case such as the one studied in this paper, the treatment of the boundary condition is very difficult to be described due to the type and quantity of IT equipment. In the interpolation method, the POD coefficients for a new design case can be also obtained by the interpolation between the weighting coefficients of the snapshots to match the new case. However, this method has been applied only for a system with less than three parameters [23] and simple geometry such as the cavity flow [42].

In the present paper, the geometry and boundary conditions for different facilities in the computation domain are complex and the order of variables' dimensions is extremely high. For the studied complicated case, we are interested in developing a steady-state temperature model in terms of multiple parameters without the need for a velocity field. In another development, machine learning methods are widely used in dealing with multi-dimensional problems, among whom the multivariate adaptive regression splines (MARS) algorithm [43–45] is a method for flexible modeling of high dimensional data, hence very suitable for the present purpose. Therefore, in this paper, the MARS is applied (realized by Python) for the weighting coefficient generation for off-design conditions. Based on the POD modes and temperature matrix, the observed weighting coefficient, denoted by $B_{i, obs}$, can be found for all snapshots by Eq. (21), which is served as one of the inputs of the MARS algorithm.

$$B_{i, obs} = \psi_i^T (T - T_0) \quad (21)$$

There are mainly two stages of the MARS algorithm: firstly, the forward pass searches for terms in the truncated power spline basis that locally minimize the squared error loss of the training set. Next, a pruning pass selects a subset of those terms that produce a locally minimal generalized cross-validation score to avoid overfitting and generate the optimal model. The weighting coefficients for a new case, b_i , are calculated through $B_{i, obs}$ of the training model between snapshots and a new operating condition.

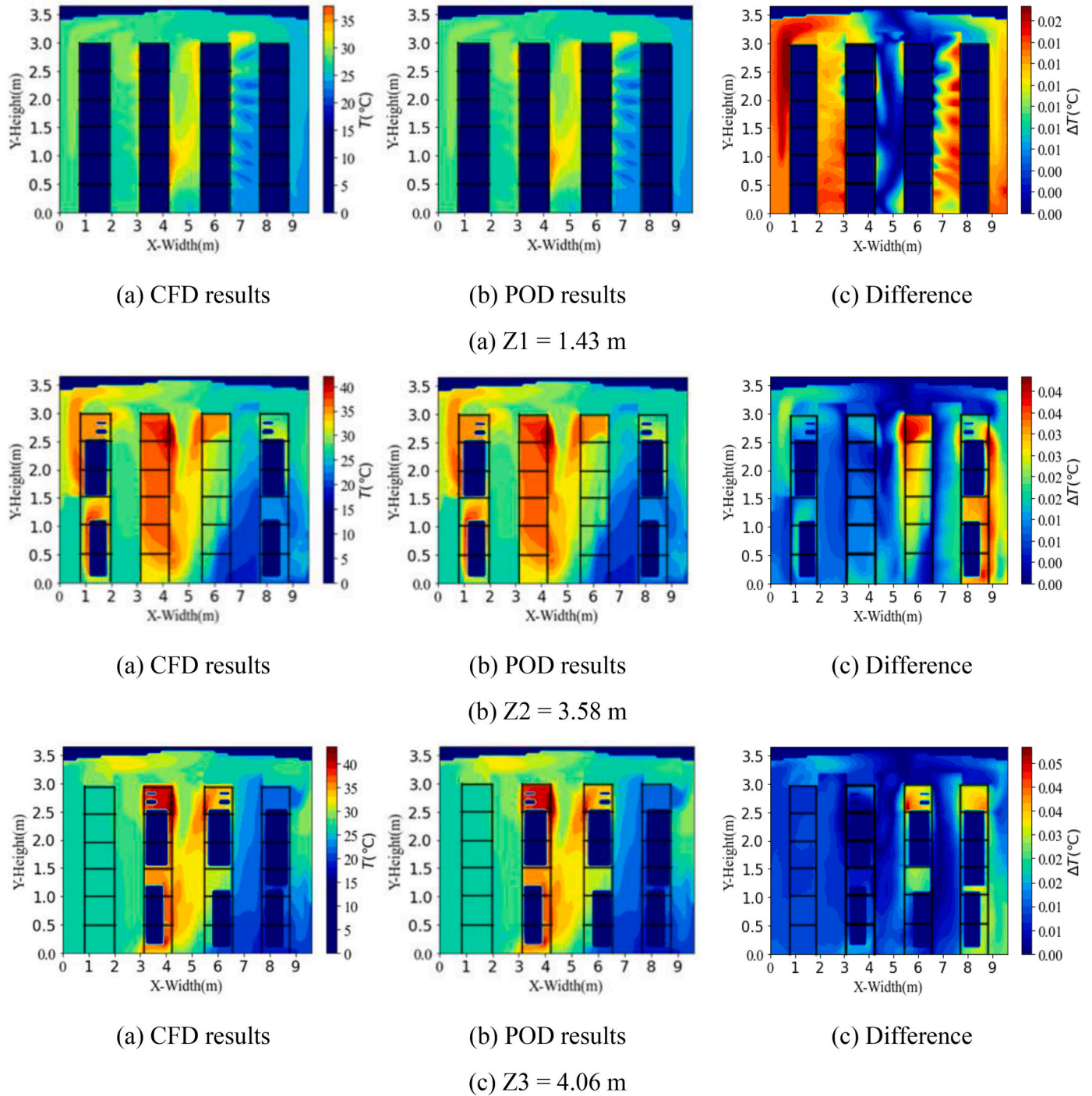


Fig. 11. Comparison of temperature contours of Z1-Z3 cross-sections between CFD simulations and POD constructions for design condition Case 1.

3.4. Temperature field construction

With calculated T_0 , ψ_b , and b_i for a new set of design variables, the corresponding temperature field can be generated from Eq. (8) through the truncated first k POD modes. To study the convergence of the obtained temperature distribution by the above POD method with a fixed number of modes and also to examine the fidelity of the POD method, the POD temperatures are compared with CFD/NHT simulations. A mean error is calculated by taking an average of the absolute and relative values of the temperature difference between POD and numerical predictions for all points, and then the average value of the total field is calculated as follows:

$$T_E(x, y, z) = |T_{POD}(x, y, z) - T_{CFD}(x, y, z)| \quad (22)$$

$$\bar{T}_E = \frac{\sum_1^{N_{nodes}} T_E(x, y, z)}{N_{nodes}} \quad (23)$$

$$T_R(x, y, z) = \frac{|T_{POD}(x, y, z) - T_{CFD}(x, y, z)|}{T_{CFD}(x, y, z)} \quad (24)$$

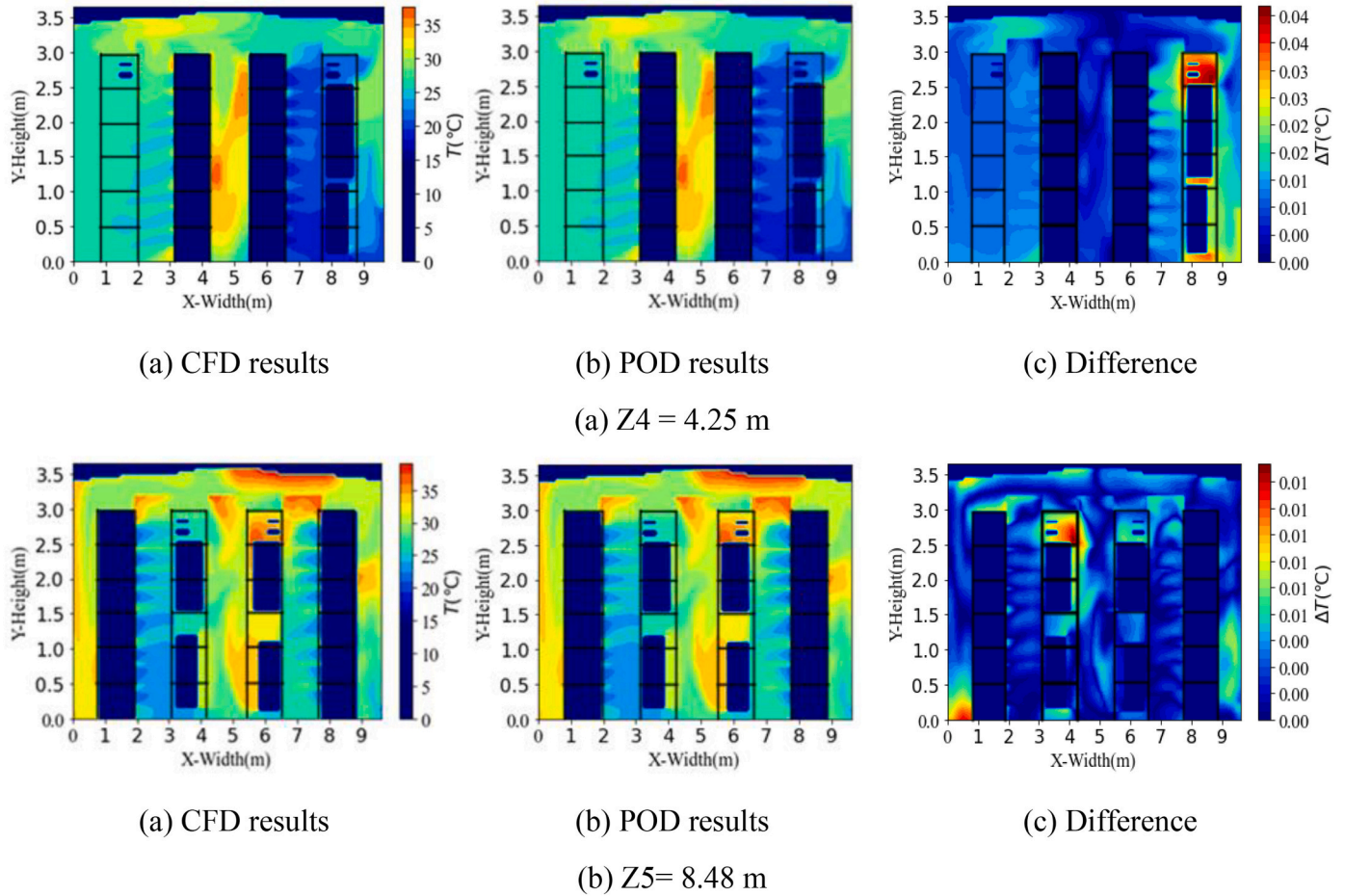


Fig. 12. Comparison of temperature contours of Z4-Z5 cross-sections between CFD simulations and POD constructions for design condition Case 1.

Table 6

Operating parameters of the off-design conditions.

No. Variable No. cases	1	2	3	...	145	146	147	148	149	...	198	199
1	350	600	3225	...	3400	225	1550	2400	19	...	900	16
2	4000	300	1900	...	1550	225	2350	2250	24	...	2550	18
3	1725	300	1375	...	1200	0	350	1200	22	...	3750	17
4	525	150	3050	...	0	75	2075	3300	26	...	3450	18
5	1900	600	1025	...	350	75	2700	1500	18	...	3000	22
6	3225	600	1900	...	1025	300	2525	3600	22	...	3750	21
7	1025	300	0	...	875	300	0	3750	25	...	0	19
8	1200	600	1375	...	3400	75	525	2400	26	...	1500	18
9	2700	450	3400	...	1375	150	2700	3450	24	...	4150	26
10	2875	600	2075	...	1900	150	3225	1200	24	...	2100	21
11	2350	0	1900	...	875	0	2075	1200	22	...	1650	22
12	525	0	525	...	2075	150	3400	3600	18	...	4400	20
13	1900	300	3600	...	2350	0	700	900	18	...	2550	24
14	1725	0	4000	...	2350	0	4000	3600	26	...	2100	21
15	1725	150	2875	...	875	150	2350	1800	19	...	2400	19
16	2700	150	875	...	1900	300	2525	1500	17	...	4150	18
17	3225	600	1900	...	1550	150	350	3600	25	...	2550	26
18	3800	600	1900	...	3050	150	2700	1800	17	...	4400	27
19	1550	300	350	...	1725	150	350	2400	16	...	1200	20
20	2075	600	1375	...	2075	300	3225	2550	24	...	1650	25

$$\bar{T}_R = \frac{\sum_1^{N_{nodes}} T_R(x, y, z)}{N_{nodes}} \quad (25)$$

where N_{nodes} is the grid cell number for the data center shown in Fig. 3.

4. Results and discussion

4.1. Verification of code for POD modes calculation

To verify the developed code for the accuracy of POD mode computation, we created the same numerical model in 6SigmaDC for the

Table 7
Results of \bar{T}_R and \bar{T}_E of 20 off-design conditions.

Case NO.	\bar{T}_R (%)	\bar{T}_E (°C)	Percentage of $T_R(x,y,z) > 15\%$	Case NO.	\bar{T}_R (%)	\bar{T}_E (°C)	Percentage of $T_R(x,y,z) > 15\%$
1	5.92	1.68	5.49	11	5.85	1.83	3.74
2	6.68	1.84	8.45	12	6.85	1.99	9.36
3	7.55	2.19	12.9	13	7.07	2.04	8.67
4	5.45	1.63	3.47	14	5.81	1.65	6.54
5	5.74	1.76	4.25	15	7.70	2.20	13.6
6	6.43	1.92	6.34	16	7.99	2.31	13.0
7	6.33	1.81	7.39	17	5.16	1.53	4.47
8	5.79	1.75	5.29	18	6.94	2.05	11.0
9	7.72	2.36	12.1	19	6.64	1.83	7.33
10	5.98	1.86	5.16	20	5.38	1.64	4.31
Mean	6.45	1.89	7.64				

case presented in the literature [16] and conducted the simulation under 21 sets of design conditions. The comparison of energy percentage captured by each mode is illustrated in Fig. 6. The energy here refers to the information captured by the POD mode [19–22]. On the whole, the two curves agree with each other well with a maximum difference of 2.88%. Therefore, our self-programming computation process of POD mode using the SVD method is reliable and can be used for the follow-up case study.

As for the present study, a total of 1819 POD modes are extracted from the snapshots of design by PICT. The energy of each POD mode can be reflected in its singular value. The POD modes are arranged according to their singular values in descending order, that is, $\sigma_1 \geq \sigma_2 \geq \sigma_3 \geq \dots \geq \sigma_{1819}$. The energy percentage captured by each POD mode is illustrated in Fig. 7. It can be noticed that for the temperature field, the tendency of energy distribution shows an exponential decline, even though the energy percentage of the first mode only accounts for about 1.35%. It means that the temperature field is complex to be captured by several POD modes because the energy percentage of each mode is relatively small. The 1268th mode represents 0.02% energy of the temperature field. After that, the energy percentage per mode can be neglected for their few contributions to the total field. The accumulated energy percentage of the first k th POD mode is shown in Fig. 8. It can be confirmed that the first 1268 POD modes capture >99.99% energy of the total temperature field.

Fig. 9 depicts the contours of six representative POD modes for the temperature field at $Z_2 = 3.58$ m cross-section where each mode 4-row racks are outlined. The contours show the normalized mode values defined by Eq.(20). This contour actually represents the temperature distribution pattern captured by the mode. For example, if only the first mode is selected in Eq.(8), then the predicted temperature distribution pattern by the POD will look like the one shown in Fig. 9(a). In Fig. 9, the scale bar shows the normalized POD mode calculated by Eq. (20), hence the absolute values are varying between 0 and 1. It indicates that the low-order POD modes depict the general distribution pattern of the temperature field and the influence of each mode is getting smaller with the increase of mode order. And the summation of enough modes with corresponding weighting coefficients will give an accurate temperature distribution for the condition studied. To guarantee the accuracy of the predicted temperature field, the truncation order of POD modes in the present study is 1268, which seems much larger than the mode number in the previous studies [20–24] where the number of modes is <10. Regarding such a large number of variables in this problem, it's necessary to use enough POD modes to contain the influence of each variable on the entire field.

4.2. Verification of developed reduced order model

In this subsection, the POD calculation formula Eq.(8) is adopted to rebuild the temperature field under design conditions and the calculation results are compared with the CFD simulation results. The results

\bar{T}_R and \bar{T}_E of the 20 sets of the designed conditions are summarized in Fig. 10. The reconstruction results show that the average mean relative error for 20 tested cases is only around 0.01%, and the mean absolute error doesn't exceed 0.01 °C.

Taking the first case as an example, temperature contours of different cross-sections from CFD simulations and POD constructions are provided in Figs. 11 and 12. The cross-sections in Z direction are selected considering different facility configurations of 4 rows. At the cross-section of $Z = 1.43$ m (Fig. 11(a)), the hot air returns into ACU in the middle hot aisle, and the same tendency can be found at the other cross-sections. The maximum difference between CFD and POD results doesn't exceed 0.02 °C.

From the temperature contours of the five cross-sections shown in Figs. 11 and 12, it can be observed that the maximum difference in local temperature between CFD simulation and POD prediction is only 0.05 °C. Therefore, POD constructions under design conditions are in very good agreement with CFD simulations. This fact confirms that the truncation order of POD modes selection is appropriate and the observed weighting coefficients are reliable.

4.3. Temperature field prediction for off-design cases

In this subsection, we aim to use the POD method for online rapid temperature field prediction under off-design conditions. The point is to obtain the weighting coefficients for any settings of 199 variables of IT equipment and ACUs. It should be noted that even though all the variables vary in the range of the design parameters shown in Table 2, it is difficult to interpolate the weighting coefficients for the solution desired directly from the weighting coefficients of the original 1819 snapshots. The truncated number of the POD modes is 1268 so the dimension of weighting coefficients is as large as [1268 × 1819]. As indicated above, the conventional interpolation methods can not deal with such a great number.

The MARS algorithm, the regression model of weighting coefficients, is adopted to compute a new series of weighting coefficients for each mode with a dimension of [1268 × 1]. Then we can directly substitute this vector into the POD calculation formula Eq.(8) with known POD modes to rebuild the temperature field for the off-design conditions.

To validate our POD method, we conduct another 20 randomly selected cases listed in Table 6 to test the proposed method. It should be indicated that among the 20 cases none of the operator parameters are the same as any of the design snapshots presented above. The detailed value for each IT equipment of the tested 20 cases can be found in Appendix.2. The POD results are compared with the CFD results in Table 7.

The results of \bar{T}_R and \bar{T}_E are summarized in Table 7. From the table, it can be seen that the average mean relative error for 20 cases is 6.45% and the mean absolute error is 1.89 °C. On average, the relative error of the three-dimensional temperature field for 92.36% doesn't exceed 15% for all the 20 off-design cases.

For the five cross-sections, the temperature contours are depicted in Figs. 13 and 14. It can be noted that in most of the computation domains, POD results are consistent with the CFD results while obvious differences occur in some local hot spot positions. The maximum error appears in the local area near the racks. At $Z = 1.43$ m cross-section, the maximum local temperature error in the hot aisle is up to 6 °C. This might be caused by the complicated flow pattern near the rack where recirculating flow usually exists. It is noteworthy that in the POD study of data center temperature distribution a local large difference often happens. For example, in Reference [17] a local error of around 8 °C was reported. Whereas, these maximum local errors account only for a little percentage of the total field. In the present study, the mean absolute error of 1.89 °C is acceptable for such a multi-variable problem in the studied data center.

It is important to compare the computational time of POD prediction and CFD simulation. A new test based on this reduced order model and

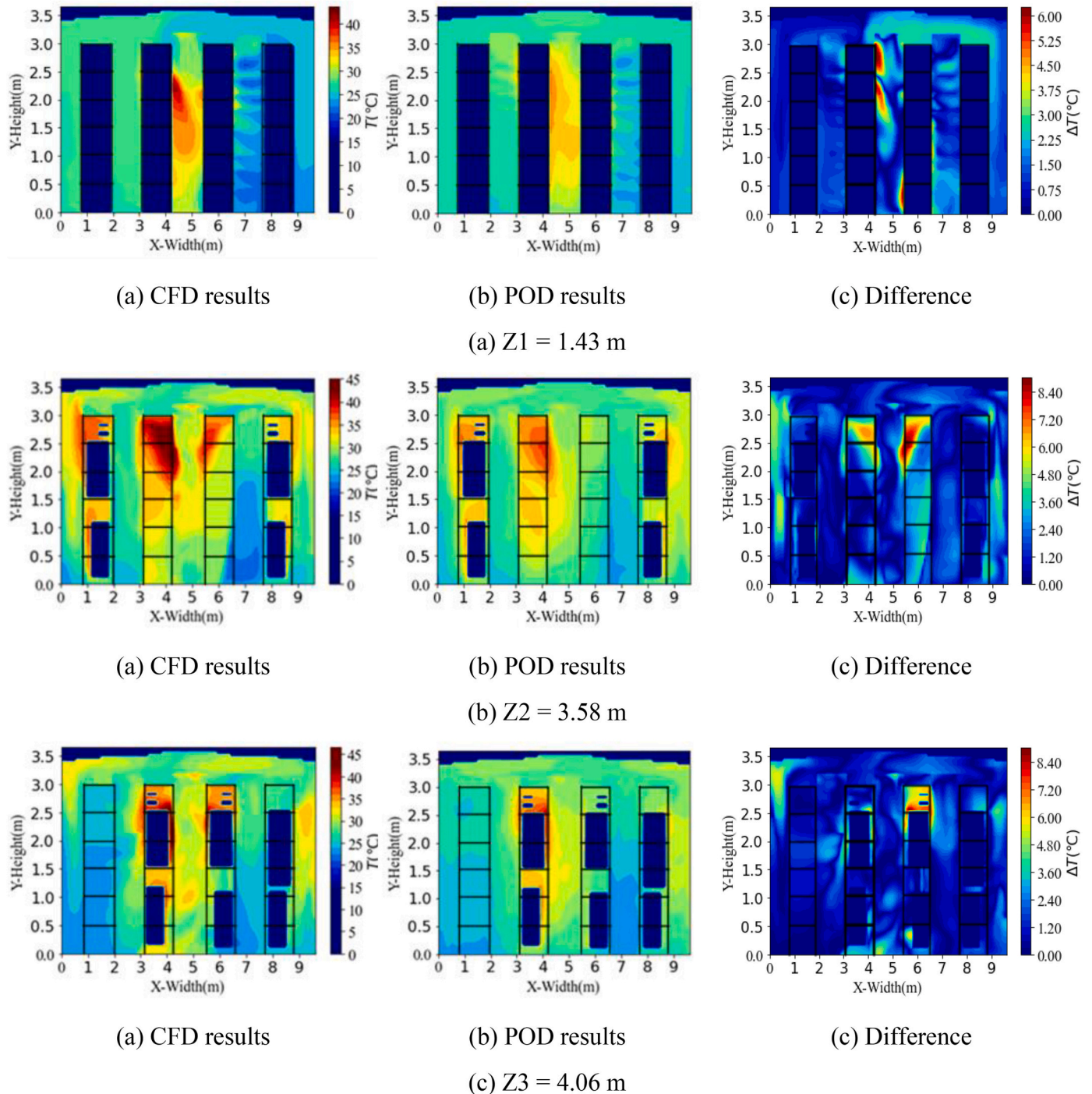


Fig. 13. Comparison of temperature contours of Z1-Z3 cross-sections between CFD simulations and POD predictions under off-design conditions.

data-driven method takes only 30s on a desktop computer (intel(R) Xeon (R) Gold5118 CPU@2.30GHz(48CPUs), 262,144 MBytes RAM). While the CFD simulation takes about 2 h to obtain the results on the same computer platform, which is nearly 240 times of the POD consumption. This fast response plays a vital role in daily operation and maintenance.

Finally, it is to be noted some of the limitations of the present POD method. First, a developed POD code can only be applied to the same data center based on which the code is developed. That is, the room layout and equipment quantities are fixed and only the changes in relevant parameters of server/air conditioning can be studied. If the physical model differs, it is necessary to recollect the datasets and reconstruct the whole procedure. Second, the accuracy of POD-MARS also

depends on the snapshots obtained by CFD simulation. Accurate CFD simulation results are the basis to get reasonably accurate POD-MARS predictions, especially for a large number of variables.

5. Conclusion

This paper investigates the approach of rapid 3D temperature field prediction for a current high-order multi-variable data center. Based on the snapshots of CFD simulations by 6SigmaDC Room, the reduced-order method POD combined with the data-driven method MARS is adopted in the present study. To the best knowledge of the authors, this paper makes the first attempt to the combination of the reduced order model

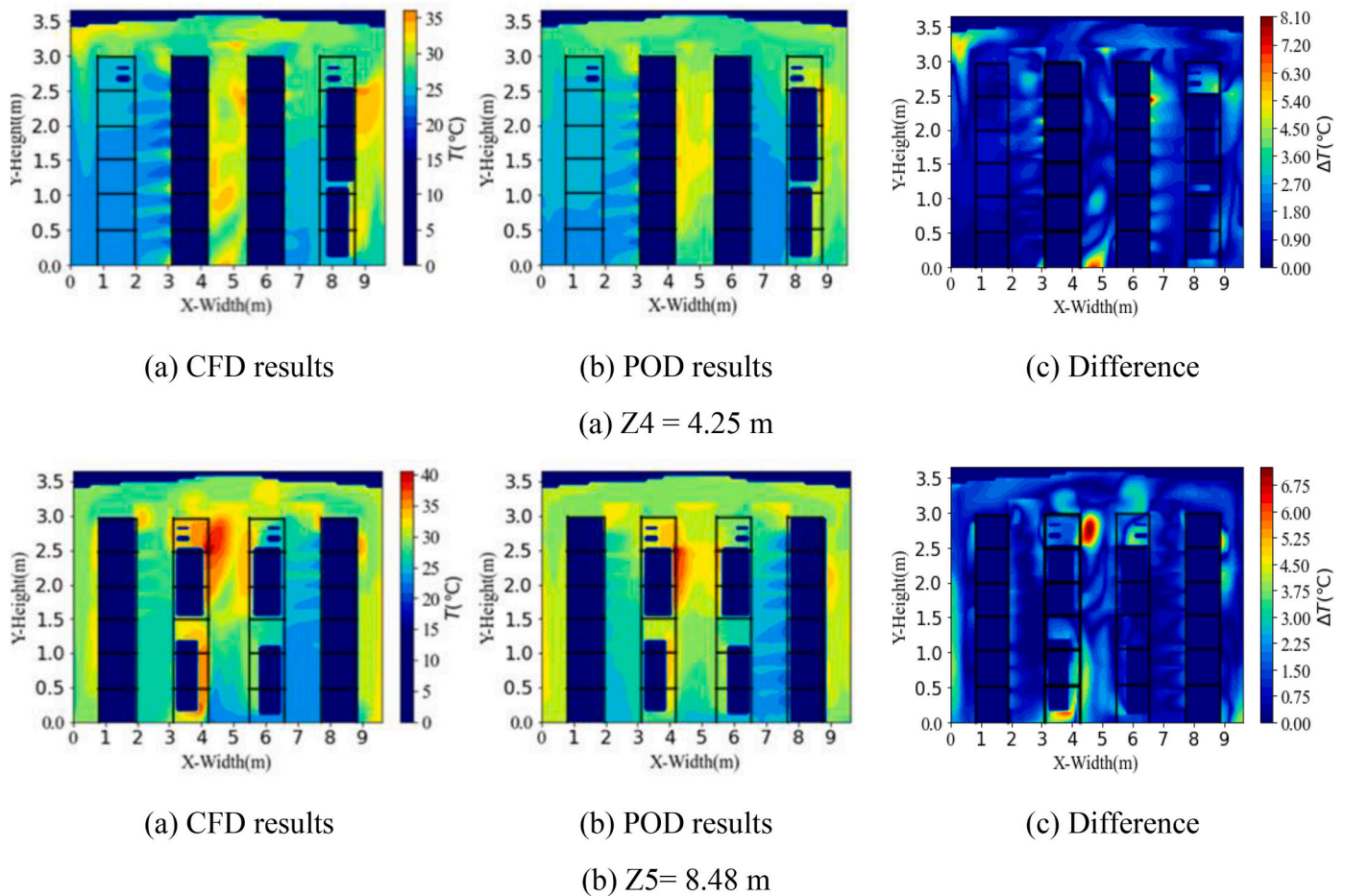


Fig. 14. Comparison of temperature contours of Z4-Z5 cross-sections between CFD simulations and POD predictions under off-design conditions.

and data-driven method in a real full-scale data center. The major works and conclusions can be summarized as follows:

- There are 199 independent variables after the 3-layer classification for racks in the present study according to the heat load of IT equipment. To maximize the amount of useful information obtained with the minimum number of experiments, a design tool called pairwise independent combinatorial testing (PICT) is applied and 1819 snapshots are generated;
- A total of 1819 POD modes are extracted using singular value decomposition (SVD) and the information captured by each POD mode is reflected in its singular value. For the temperature field, the tendency of energy distribution shows an exponential decline, while the energy percentage of each mode is relatively dispersed which means that the temperature field is complex to be captured by several POD modes. Therefore, the truncation order of POD modes is 1268 through which 99.99% of total energy can be captured;
- POD constructions under design conditions are in good agreement with CFD simulations, the average mean relative error for 20 tested cases is about 0.01%, and the mean absolute error doesn't exceed 0.01 °C. The maximum relative error is 0.02%;
- For the rapid temperature field prediction under off-design conditions, 20 cases are designed randomly and their total temperature fields are calculated by CFD simulation and POD-MARS computation, respectively. The average mean relative error for 20 cases is 6.45% and the mean absolute error is 1.89 °C. On average, the relative error for 92.36% of the three-dimensional temperature field doesn't exceed 15%. Even though some local

relatively-large error occurs, they account for a little percentage of the total field and the general results are acceptable for such a multi-variable problem in the studied real data center;

- As for the computational time cost, the POD-MARS computation takes only 30s to obtain the POD temperature field for the same test case which is ~240 times faster than the CFD simulation on the same computing platform. It should be noted that the preparation of test design, the collection of datasets, and the training of datasets will need plenty of offline time to ensure the final online rapid computation.

Author statement

Shu-Qi Jin: Investigation, Writing – original draft, Writing – review & editing, Visualization;

Nan Li: Investigation, Methodology, Validation;

Fan Bai: Investigation, Methodology, Validation;

Yu-Jie Chen: Investigation, Methodology, Validation;

Xiang-You Feng: Investigation, Data curation

Hao-Wei Li: Investigation, Visualization;

Xiao-Ming Gong: Investigation, Validation;

Wen-Quan Tao: Conceptualization, Resources, Writing – review & editing, Supervision, Project administration, Funding acquisition.

We confirm that the final submitted manuscript has been shared with all authors listed on the manuscript and that all authors have confirmed their agreement to the manuscript.

Declaration of Competing Interest

The authors declare that they have no known competing financial interests or personal relationships that could have appeared to influence the work reported in this paper.

Data availability

Data are provided in the Appendix.

Acknowledgment

This work is supported by the Foundation for Innovative Research Groups of the National Natural Science Foundation of China (No.51721004), the NSFC-STINT (Energy Management of Fuel Cell Powered Data Centers)(51911530157), the Fund of Xi'an Science and Technology Bureau (20192187 14SYS002CG024), and the 111 Project (B16038).

Appendix. Supplementary data

Supplementary data to this article can be found online at <https://doi.org/10.1016/j.icheatmasstransfer.2023.106645>.

References

- [1] Y. Joshi, P. Kumar, *Energy Efficient Thermal Management of Data Centers*[M], Springer Science + Business Media, New York, USA, 2012.
- [2] A. Almoli, A. Thompson, N. Kapur, J. Summers, H. Thompson, G. Hannah, Computational fluid dynamic investigation of liquid rack cooling in data centres, *Appl. Energy* 89 (1) (2012) 150–155.
- [3] X. Qian, Z. Li, Z. Li, A thermal environmental analysis method for data centers, *Int. J. Heat Mass Transf.* 62 (2013) 579–585.
- [4] K. Karki, A. Radmehr, S. Patankar, Use of computational fluid dynamics for calculating flow rates through perforated tiles in raised-floor data centers, *HVAC&R Res.* 9 (2) (2003) 153–166.
- [5] S.V. Patankar, Airflow and cooling in a data center, *ASME J. Heat Transf.* 132 (7) (2010).
- [6] H. Fernando, J. Siriwardana, S. Halgamuge, Can a data center heat-flow model be scaled down?, in: *IEEE International Conference on Information & Automation for Sustainability*, 2013.
- [7] Z. Song, B.T. Murray, B. Sannakia, Numerical investigation of inter-zonal boundary conditions for data center thermal analysis, *Int. J. Heat Mass Transf.* 68 (2014) 649–658.
- [8] S.A. Nada, M.A. Said, M.A. Rady, CFD investigations of data centers' thermal performance for different configurations of CRACs units and aisles separation, *Alexandria Eng. J.* 55 (2) (2016) 959–971.
- [9] S.A. Nada, M.A. Said, Effect of CRAC units layout on thermal management of data center, *Appl. Therm. Eng.* 118 (2017) 339–344.
- [10] X. Gong, Z. Zhang, S. Gan, B. Niu, L. Yang, H. Xu, M. Gao, A review on evaluation metrics of thermal performance in data centers, *Build. Environ.* 177 (2020), 106907.
- [11] A.M. Abbas, A.S. Huzayyin, T.A. Mouneer, S.A. Nada, Thermal management and performance enhancement of data centers architectures using aligned/staggered in-row cooling arrangements, *Case Stud. Therm. Eng.* 24 (2021), 100884.
- [12] L. Phan, C.X. Lin, M. Telusma, Asme, data center modeling using response surface with multi-parameters approach, in: *Proceedings of the ASME International Mechanical Engineering Congress and Exposition*, 2016.
- [13] J.W. VanGilder, Z.R. Sheffer, X.H. Zhang, C.M. Healey, Ashrae, Potential Flow Model for Predicting Perforated Tile Airflow in Data Centers, *ASHRAE Transactions*, 2011, pp. 771–786.
- [14] E. Cruz, Y. Joshi, Inviscid and viscous numerical models compared to experimental data in a small data center test cell, *J. Electron. Packag.* 135 (3) (2013).
- [15] J. Lumley, *The Structure of Inhomogeneous Turbulent Flows*. Atmospheric Turbulence and Radio Wave Propagation, 1967.
- [16] P. Ding, X. Wu, Y. He, W. Tao, A fast and efficient method for predicting fluid flow and heat transfer problems, *ASME J. Heat Transf.* 130 (3) (2008).
- [17] D. Han, B. Yu, J. Chen, Y. Wang, Y. Wang, POD reduced-order model for steady natural convection based on a body-fitted coordinate, *Int. Commun. Heat Mass Transf.* 68 (2015) 104–113.
- [18] J. Chen, D. Han, B. Yu, D. Sun, J. Wei, A POD-Galerkin reduced-order model for isotropic viscoelastic turbulent flow, *Int. Commun. Heat Mass Transf.* 84 (2017) 121–133.
- [19] T. Li, D. Han, B. Yu, J. Li, D. Sun, Study on a POD reduced-order model for steady-state flows in fractured porous media, *Int. Commun. Heat Mass Transf.* 112 (2020).
- [20] E. Samadiani, Y. Joshi, Proper orthogonal decomposition for reduced order thermal modeling of air cooled data centers, *ASME J. Heat Transf.* 132 (7) (2010), 071402.
- [21] E. Samadiani, Y. Joshi, Multi-parameter model reduction in multi-scale convective systems, *Int. J. Heat Mass Transf.* 53 (9–10) (2010) 2193–2205.
- [22] E. Samadiani, Y. Joshi, H. Hamann, M.K. Iyengar, S. Kamalsy, J. Lacey, Reduced order thermal modeling of data centers via distributed sensor data, *ASME J. Heat Transf.* 134 (4) (2012).
- [23] R. Ghosh, Y. Joshi, Rapid temperature predictions in data centers using multi-parameter proper orthogonal decomposition, *Num. Heat Transf. Part A: Appl.* 66 (1) (2014) 41–63.
- [24] L. Phan, C.-X. Lin, Reduced order modeling of a data center model with multi-parameters, *Energy Build.* 136 (2017) 86–99.
- [25] J.D. Moore, J.S. Chase, P. Ranganathan, Weatherman: automated, online and predictive thermal mapping and management for data centers, in: *2006 IEEE International Conference on Autonomic Computing*, IEEE, Dublin, Ireland, 2006.
- [26] F. Ahmad, T.N. Vijaykumar, Joint optimization of idle and cooling power in data centers while maintaining response time, *ACM* (2010) 243.
- [27] K. Fouladi, A.P. Wemhoff, L. Silva-Llanca, K. Abbasi, A. Ortega, Optimization of data center cooling efficiency using reduced order flow modeling within a flow network modeling approach, *Appl. Therm. Eng.* 124 (2017) 929–939.
- [28] J. Athavale, M. Yoda, Y. Joshi, Comparison of data driven modeling approaches for temperature prediction in data centers, *Int. J. Heat Mass Transf.* 135 (2019) 1039–1052.
- [29] S. Asgari, H. Moazamigoodarzi, P.J. Tsai, S. Pal, R. Zheng, G. Badawy, I.K. Puri, Hybrid surrogate model for online temperature and pressure predictions in data centers, *Futur. Gener. Comput. Syst.* 114 (2021) 531–547.
- [30] S. Asgari, S. MirhoseiniNejad, H. Moazamigoodarzi, R. Gupta, R. Zheng, I.K. Puri, A gray-box model for real-time transient temperature predictions in data centers, *Appl. Therm. Eng.* 185 (2021).
- [31] L. Phan, C.-X. Lin, CFD-based response surface methodology for rapid thermal simulation and optimal design of data centers, *Adv. Build. Energy Res.* 14 (4) (2020) 471–493.
- [32] C. Jin, X. Bai, C. Yang, Effects of airflow on the thermal environment and energy efficiency in raised-floor data centers: a review, *Sci. Total Environ.* 695 (2019), 133801.
- [33] S.K. Shrivastava, A.R. Calder, M. Ibrahim, Quantitative comparison of air containment systems, in: *13th InterSociety Conference on Thermal and Thermomechanical Phenomena in Electronic Systems*, 2012, pp. 68–77.
- [34] H. Hotelling, Analysis of a complex of statistical variables in principal components, *J. Educ. Psychol.* 24 (7) (1933) 498–520.
- [35] A. Pentl, B. Moghaddam, T. Starner, View-based and modular eigenspaces for face recognition, in: *Proceedings / CVPR, IEEE Computer Society Conference on Computer Vision and Pattern Recognition*, 1994.
- [36] M. Loève, *Probability Theory II*, 4th ed, Springer-Verlag, 1978.
- [37] R. Mukerjee, C.F.J. Wu, *A Modern Theory of Factorial Designs*, Springer, New York, 2006.
- [38] R. Liu, Y. Zhang, C. Wen, J. Tang, Study on the design and analysis methods of orthogonal experiment, *Exp. Technol. Manag.* 27 (09) (2010) 52–55.
- [39] K.C. Tai, Y. Lei, A test generation strategy for pairwise testing, *IEEE Trans. Softw. Eng.* 28 (1) (2002) 109–111.
- [40] K. Fang, D.K.J. Lin, P. Winker, Y. Zhang, Uniform design: theory and application, *Technometrics* 42 (3) (2002) 237–248.
- [41] J. Demmel, K. Veseli, Jacobis method is more accurate than QR, *SIAM J. Sci. Stat. Comput.* 13 (1992).
- [42] Y. Wang, B. Yu, Z.Z. Cao, W.Z. Zou, G.J. Yu, A comparative study of POD interpolation and POD projection methods for fast and accurate prediction of heat transfer problems, *Int. J. Heat Mass Transf.* 55 (17–18) (2012) 4827–4836.
- [43] J.H. Friedman, Multivariate adaptive regression spline, *Ann. Stat.* 19 (1) (1991).
- [44] J.H. Friedman, C.B. Roosen, An introduction to multivariate adaptive regression splines, *Stat. Methods Med. Res.* 4 (3) (1995) 197–217.
- [45] N. Rolander, *An Approach for the Robust Design of air Cooled Data Center Server Cabinets*, Georgia Institute of Technology, Atlanta, GA, 2005.